Science of the Total Environment 981 (2025) 179598

Contents lists available at ScienceDirect

Science of the Total Environment

journal homepage: www.elsevier.com/locate/scitotenv

Hyperspectral characterization of wastewater in the Tijuana River Estuary using laboratory, field, and EMIT satellite spectroscopy

Eva Scrivner [a,*,1], Natalie Mladenov [b], Trent Biggs [a], Alexandra Grant [b], Elise Piazza [a], Stephany Garcia [a], Christine M. Lee [c], Christiana Ade [c], Nick Tufillaro [d], Philipp Grötsch [d], Omar Zurita [d], Benjamin Holt [c], Daniel Sousa [a]

[a] Department of Geography, San Diego State University, San Diego, CA, USA
[b] Department of Civil, Construction, and Environmental Engineering, San Diego State University, San Diego, CA, USA
[c] Jet Propulsion Laboratory, California Institute of Technology, Pasadena, CA, USA
[d] Gybe, Corvallis, OR, USA

HIGHLIGHTS

- Reflectance spectra of Tijuana River wastewater dilutions contain a 620 nm spectral dependency.
- The depth of this feature is highly correlated with paired water quality parameters ($R^2 \geq 0.97$, p-value < 0.01)
- One of the first applications of EMIT imagery for water quality utility is presented.
- Future algorithms may be fitted to remotely retrieve water quality parameters that co-vary with this spectral feature.

GRAPHICAL ABSTRACT

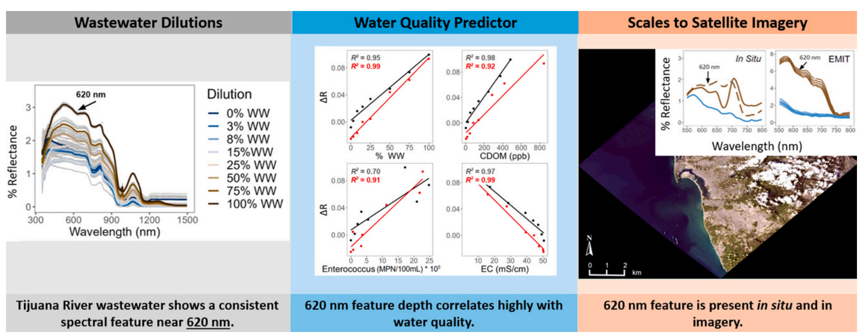

ARTICLE INFO

Editor: Jay Gan

Keywords:
Bacterial contamination
Coastal and inland waters
Tijuana River
Reflectance spectroscopy
EMIT

ABSTRACT

Hundreds of millions of liters of untreated wastewater are discharged into the Tijuana River annually, impacting communities on both sides of the US-Mexico border. Current monitoring methods are resource-intensive and limited in coverage. Optical satellite imaging may enable broader spatiotemporal monitoring, yet retrievals of bacterial concentrations and other key water quality indicators remain challenging. Here we investigate the utility of spectroscopic sensors to monitor the presence of wastewater in this estuarine-coastal system, as a proxy for bacterial concentrations and other water quality parameters. We prepared dilutions of untreated wastewater and uncontaminated seawater, measuring visible through shortwave infrared (VSWIR; 350–2500 nm) reflectance spectra of each sample. At high wastewater concentrations, a distinct spectral feature centered near 620 nm strongly correlated with paired water quality measurements ($R^2 \geq 0.97$, p-value < 0.01). This feature is additionally observed in multispectral resolution, in field observations, and in hyperspectral satellite imagery. An example application of plume mapping with this feature is presented, representing one of the earliest adoptions of EMIT hyperspectral satellite imagery for water quality monitoring. These results are promising for the use of

* Corresponding author at: Department of Geography, 5500 Campanile Drive, SH-314, San Diego, CA 92182-4493, USA.
E-mail address: mel24004@uconn.edu (E. Scrivner).
[1] Present address: Department of Marine Sciences, 1080 Shennecossett Road, Groton, CT 06340, USA.

https://doi.org/10.1016/j.scitotenv.2025.179598
Received 26 September 2024; Received in revised form 1 May 2025; Accepted 1 May 2025
Available online 8 May 2025

spectroscopic sensors to map and monitor wastewater pollution in the Tijuana River Estuary and potentially, similarly polluted coastal and estuarine systems.

1. Introduction

Hundreds of millions of liters of treated and untreated wastewater have been expelled into the binational Tijuana River each year (International Boundary and Water Commision, 2020; Ayad et al., 2020; McLamb et al., 2024). Discharging from the overburdened Tijuana sewage system, this water carries harmful pollutants through two major cities (over 3 million combined residents), as well a protected estuarine reserve (Tijuana River National Estuarine Research Reserve, 2020; Calderón-Villarreal et al., 2022). When cross-border flows were infrequent, costs of hazardous material removal were an estimated $900,000 (California-Mexico Border Relations Council, 2017), in addition to the $1.8 million already directed to annual maintenance (Tijuana River National Estuarine Research Reserve, 2020). More recently, chronic untreated sewage flow in the Tijuana River started in October 2022 and has continued without pause at the time of writing, resulting in continuous beach closures in adjacent Imperial Beach, with significant impacts on the economy, health, and quality of life (Feddersen et al., 2021). Efforts to improve wastewater management in the Tijuana River system are ongoing; the U.S. and Mexican governments have approved a plan to jointly contribute nearly $500 million to improve infrastructure by 2027 (International Boundary and Water Commision, 2022). A pressing need clearly exists for effective mapping and monitoring of wastewater pollution in this area, as well as similar areas worldwide.

Water quality in the Tijuana River Estuary is routinely monitored using water sampling and stationary sondes. Sampling campaigns are laborious and resource intensive, requiring extensive planning and personnel, limiting their frequency. Multiparameter sondes are used to complement these grab samples, allowing for continuous (10-min) monitoring at sites of interest (Fig. 1). Such sondes operate at fixed locations, limiting spatial coverage. *In situ* samples provide an invaluable and detailed record of water quality, but important observational gaps remain in both space and time. Satellite imaging provides a potentially valuable source of complementary observations which could help fill data gaps between *in situ* measurements — if the water quality parameters of interest could be reliably retrieved.

One promising recent advance in water quality monitoring of the area has incorporated the use of *in situ* fluorescence spectroscopy. Microbial activity has been demonstrably correlated with "Peak T" fluorescence, a fluorescent peak, occurring at an excitation (absorption) wavelength of 275 nm and an emission wavelength of ~340 nm, named after its similarity to the signature of the amino acid tryptophan (Coble, 1996). The intensity of the Peak T fluorescence signal in three-dimensional excitation and emission matrices (EEM) can be a strong predictor of a variety of water quality parameters, including Biological Oxygen Demand (BOD) (Hudson et al., 2008), percent wastewater (Goldman et al., 2012), and *E. coli* bacterial concentrations (Sorensen et al., 2015; Sorensen et al., 2020). While the Peak T signal is not retrievable by remote sensors, optical signals characteristic of untreated wastewater may also exist. Historical analysis of multispectral imagery (Ayad et al., 2020) shows intriguing wastewater signatures based on remote sensing of chromophoric dissolved organic matter (CDOM). If diagnostic and generalizable optical indicators of bacterial contamination can be found, it might be possible to directly map wastewater plumes from satellite imagery with high accuracy and precision.

Decades of previous studies have used optical signatures to characterize water quality parameters in other coastal environments (*e.g.* Seyhan and Dekker, 1986; Dekker, 1993; Kallio et al., 2001; Brando and Dekker, 2003; Giardino et al., 2007). Previously retrieved water parameters include but are not limited to Chlorophyll-a in open ocean and coastal systems (*e.g.* Gordon and Morel, 1983; Gemperli, 2004), Chromophoric Dissolved Organic Matter (CDOM) (*e.g.* Lee et al., 2002; Aurin

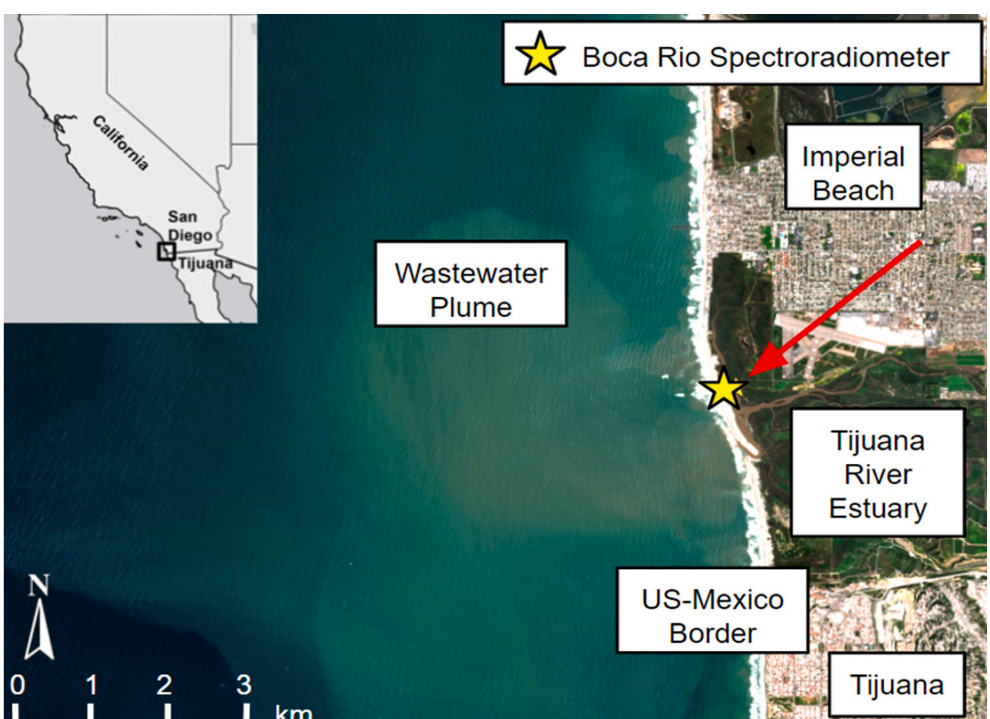

Fig. 1. True color Sentinel-2 image of the Tijuana River Estuary and coastal ocean. This image (collected on 24 March 2023) captures a wastewater plume. Location of field deployed spectroradiometer is indicated with a yellow star.

et al., 2018), turbidity (*e.g.* Myint and Walker, 2002; Nechad et al., 2010), and select bacterial parameters (*e.g.* Grimes et al., 2014; Cheng et al., 2022). Optical retrievals generally leverage reflectance spectra at visible through shortwave infrared (SWIR; approx. 400–2500 nm) wavelengths, capitalizing on absorption features and other optical signals created by accessory pigments, back scattering, and more. In the Tijuana River Estuary, wastewater plumes and stormwater runoff have already been effectively characterized using multispectral and synthetic aperture radar (SAR) satellite observations (Ayad et al., 2020), as well as in other Southern California coastal systems (Bay et al., 2003; DiGiacomo et al., 2004; Holt et al., 2017; Gierach et al., 2017). While these studies successfully classify plume presence and type, further work is necessary to model finer-scale water quality parameters with higher accuracy and to effectively scale up existing monitoring efforts in the Tijuana Estuary.

Here we investigate the potential for recent advances in field and satellite imaging spectroscopy to improve our ability to map and monitor wastewater pollution in the Tijuana River Estuary. We prepared dilutions of pure untreated wastewater into clean distal seawater collected on two dates. We characterize a wide range of water constituents (tryptophan, CDOM, turbidity, electric conductivity, *Escherichia coli*, total *Enterococcus*, total coliforms, COD, DOC, and Total Dissolved Nitrogen (TDN)) for each dilution, while also collecting paired VSWIR reflectance spectra. We address the following fundamental questions: 1) What, if any, characteristic spectral features exist in "pure" and mixed wastewater? 2) How do any features correlate with independently measured water quality like bacteria concentrations and CDOM? and 3) Can we scale to spaceborne measurements and begin to elucidate spatial patterns in wastewater signal in coastal environments? Results suggest the existence of a spectral feature centered near 620 nm which appears to scale linearly with key water quality parameters and may be a promising tool for ongoing monitoring in the study area.

2. Background

For more than four decades, remote sensing methods have been widely applied for routine water quality monitoring and analysis (*e.g.* Seyhan and Dekker, 1986; Dekker, 1993; Kallio et al., 2001; Brando and Dekker, 2003; Giardino et al., 2007). This is possible due to the interactions of light with optically active water constituents, which impact observed spectral radiation through absorption and scattering of light. These spectral features, particularly in the VSWIR region, can be used to develop algorithmic retrievals of relevant water quality parameters (WQPs). Extensive research has already been conducted to characterize and model optically active WQPs. Additional estimates of non-optically active parameters have been conducted by leveraging statistical relationships with other optically active constituents. This has been attempted for retrievals of BOD (*e.g.* He et al., 2009), COD (*e.g.* Miao-fen et al., 2007; He et al., 2009), and DOC (*e.g.* Mannino et al., 2008; Tehrani et al., 2013). The relationship of these parameters with spectral reflectance remains poorly characterized, however (Gholizadeh et al., 2016). Further relevant water quality indicators including pH and Total Dissolved Nitrogen (TDN) are also largely absent in the literature, with weak optical signals or poor signal-to-noise proving difficult to circumvent (Gholizadeh et al., 2016).

Chlorophyll-a (chl-a), a well characterized WQP, is the primary photosynthetic pigment and is associated with eutrophication, algal blooms, productivity, and phytoplankton biomass. When recorded in living tissue, chl-a absorption spectra characteristically peak at high energy blue wavelengths centered near 440 nm and red wavelengths centered at 675 nm (Bidigare et al., 1990, Bricaud et al., 1995, Ciotti et al., 2002). This is true globally across both terrestrial and aquatic systems. An increase in chl-a concentrations results in a decrease in reflectance magnitudes at blue bands in the 400–500 nm range (Ritchie et al., 1990; George, 1997; Brivio et al., 2001). In open ocean systems, chl-a concentrations are commonly retrieved using this high blue-green absorption (Gordon and Morel, 1983). However, in coastal, optically dynamic systems this blue-green feature is obscured due to absorption of other dissolved organic molecules (Miller et al., 2002). Thus, more complex optical models are employed, many of which leverage high absorption at 675 nm to model chl-a in turbid waters (Gitelson et al., 2008).

Chromophoric dissolved organic matter (CDOM) refers to light absorbing DOM, with CDOM sensors particularly tracking the humic like fluorescence of brown heterogenous dissolved organic molecules present in freshwater and coastal saline systems. Generally, CDOM has high absorption at high energy UV and blue wavelengths, with absorption decreasing exponentially across the VSWIR spectrum (*e.g.* Jerlov, 1968; Kirk, 1976; Visser, 1984). This holds true across diverse global aquatic and marine systems (Kirk, 1976; Grunert et al., 2018). The co-occurrence of CDOM and Chl-a absorption at high energy blue wavelengths convolutes global Chl-a algorithms in coastal systems, and many algorithms circumvent this by tuning to red band absorption (*e.g.* Moses et al., 2009; Gitelson et al., 2009). As such, more complex, regionally tuned models are often necessary to accurately model chl-a in optically complex, CDOM-rich coastal waters (*e.g.*, Freitas and Dierssen, 2019).

Given the need to inform public health and policy, understanding the spatial distribution of bacterial parameters, particularly in nearshore environments, are in high demand, yet direct retrievals from remote sensing reflectance remain a challenge. Previous studies have modeled optically active harmful bacteria, such as cyanobacteria, by leveraging absorption features created by accessory pigments. Accessory pigments support photosynthesis in an organism by extending the range of absorbable wavelengths. In the case of cyanobacteria, the accessory pigment phycocyanin has a documented high absorption centered at 620 nm; this has been leveraged to estimate cyanobacteria in polluted aquatic systems (Simis et al., 2005; Simis et al., 2006; Dominguez Gómez et al., 2008; Randolph et al., 2008). However, non-optically active bacterial parameters present more of a challenge. One study suggests the feasibility of modeling *Enterococcus* concentrations through satellite remote sensing, though correlations are only moderately accurate (Zhang et al., 2010). However, to our knowledge, few other studies have explored remote retrievals of *Enterococcus*. *E. coli* concentrations are similarly under-characterized yet highly relevant for water quality monitoring. One study deployed a Radon-222 tracer to overcome the lack of *E. coli* optical characteristics, allowing for detection with UAV thermal imagery (Cheng et al., 2022). While allowing for effective retrieval of *E. coli* concentrations, this method is resource intensive and may not be applicable for all contexts. Other studies have employed machine learning techniques to model *E. coli* concentrations with varying degrees of accuracy (Morgan et al., 2021). In sum, remote retrievals of non-optically active bacterial parameters, such as through the use of co-varying statistical relationships, are an ongoing area of research.

Tryptophan, a key amino acid, has a well-documented high correlation with *E. coli* in wastewater-contaminated aquatic systems. Under nutrient limited conditions, *E. coli* secrete dissolved tryptophan molecules as they transit to a more dormant state (Arana et al., 2004). As a result, measurement of UV tryptophan-like fluorescence is a strong indicator of *E. coli* contamination (Sorensen et al., 2015), and fluorescence methods have been used to successfully model *E. coli* in various wastewater-contaminated systems through *in situ* methods (Mendoza et al., 2020; Nowicki et al., 2021; Ward et al., 2021; Dapkus et al., 2023). To our knowledge, little to no remote sensing retrievals of tryptophan concentrations exist in the literature. Accurate remote retrievals of tryptophan may prove effective in indirectly deriving bacterial parameters and circumventing a lack of optical signature.

3. Methods

3.1. Data collection

On 26 October 2023 and 14 February 2024, samples of untreated wastewater (WW) were retrieved from the South Bay International Wastewater Treatment Plant in San Diego, CA, USA (33.001509° N, 117.278600° W) and transported to the San Diego State University campus, along with same-day samples of seawater (SW) collected from Cardiff State Beach (33.001509° N, 117.278600° W). Seawater samples were collected between 8:00 am and 9:00 am Local Standard Time on the experiment date; the October sample was collected during the onset of ebb tide while the February sample was collected during flood tide. Dilutions were conducted by adding wastewater to seawater to create 1 L samples of the following concentrations: 0 % WW (pure seawater), 3 %, 8 %, 15 %, 25 %, 50 %, 75 %, and 100 % WW (pure wastewater). Smaller subsamples of these 1 L batches were collected and used separately for measurement by a HORIBA Aqualog® benchtop fluorometer and a Spectra Vista Corporation™ (SVC) HR-1024i spectroradiometer.

Three-dimensional excitation emission matrix spectra (EEMs) of the filtered samples (0.7 μm glass fiber filter) placed inside a quartz cuvette (path length of 1 cm) were acquired using a Horiba Aqualog Spectrofluorometer reading excitation wavelengths from 240 to 450 nm and emission wavelengths from 300 to 560 nm at a 0.25 s integration time. Other instrument settings and corrections (blank subtraction, Raman normalization, and Rayleigh masking) are described in Mendoza et al., 2020. The intensities of TRP and CDOM peaks were recorded in Raman units (RU) and converted to ppb TRP (1 RU = 50.8 ppb TRP) and ppb CDOM (1 RU = 143.4 ppb CDOM) using calibration curves with tryptophan and quinine sulfate standards. All water quality measurements from the October and February experiments, including for pure seawater and wastewater samples, are presented in the Supplementary Materials (Tables S1, S2).

Reflectance spectra of the unfiltered sample dilutions were collected under controlled laboratory conditions using an SVC HR-1024i spectroradiometer from 300 to 2500 nm. Samples were illuminated by a tungsten halogen lamp (Fig. 2). Instrument noise equivalent radiance is reported as $\leq 0.8 \times 10^{-9}$ W/cm^2/nm/sr at 700 nm, $\leq 1.2 \times 10^{-9}$ W/cm^2/nm/sr at 1500 nm, and $\leq 1.2 \times 10^{-9}$ W/cm^2/nm/sr at 2100 nm. Band spacing is 1.5 nm from 350 to 1000 nm, 3.8 nm from 1000 to 1890 nm, and 2.5 nm from 1890 to 2500 nm (Spectra Vista Corporation, 2012). Measurements were collected using an armored fiber optic with a 25° field of view. The operator held the fiber optic tip within a pistol grip oriented 45° from nadir such that the entire field of view only included the target sample and 130° from the light source to minimize self-shadowing and glint following Mobley, 1999. Radiance measurements of a Spectralon white reference plaque were collected approximately 30 s prior to collecting 10 radiance measurements of each sample dilution, contained in a one-liter matte black container filled to the brim. Sample radiances were divided by plaque radiances to compute final reflectance spectra for each sample (Fig. 3). Reference reflectance spectra of the matte black container were also recorded using an SVC Leaf Clip and Reflectance Probe (LC-RP) contact probe placed flush with the container (Fig. 3).

Of note, the matte black container used in spectral data collection is shallow with high internal scattering expected off the sides and bottom of the container. As such, the influence of the container on recorded reflectance will be greatest in distal seawater samples. The container reflectance spectra are presented below (Fig. 3), and the downwelling irradiance of the tungsten halogen lamp light source is presented in the Supplementary Materials (Fig. S1). As the wastewater concentration increases, high particulate scattering will reduce the signal of the vessel such that both the signal of wastewater and seawater are more pronounced. The observational scenario with which we made these measurements was the result of several months of discussion about the limitations of our hardware and legal restrictions related to the handling

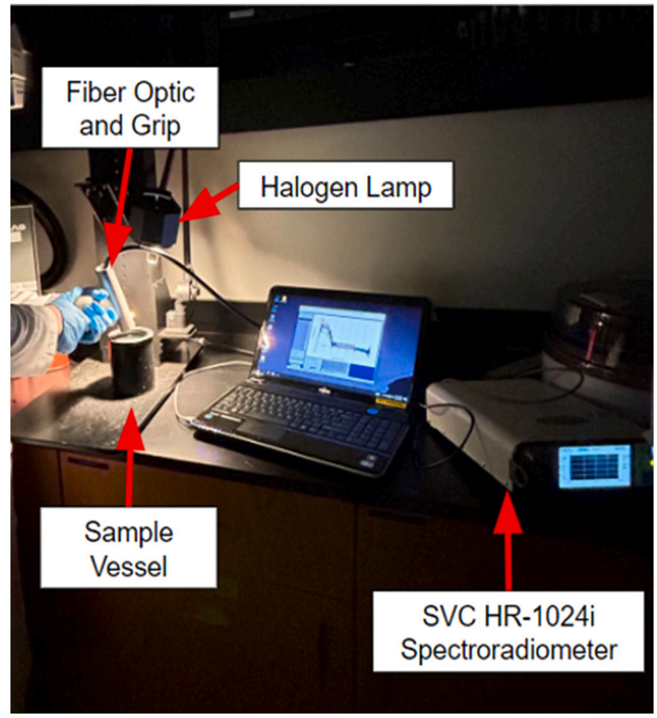

Fig. 2. Experimental setup used for both wastewater addition experiments on 10/26/2023 and 02/14/2024. Samples were contained in an open, matte black container and illuminated solely by a tungsten halogen lamp. Container was approximately spectrally flat, with maximum reflectance of 2 %. The fiber optic tip was held within a pistol grip, oriented approximately 130° from the light source and 45° from nadir to minimize self-shadowing and glint following Mobley (1999).

of hazardous untreated wastewater, though we acknowledge future work may build upon these findings using a larger vessel to reduce amplified forward scattering by the container.

3.2. Spectral analysis

Reflectance anomalies, also known in the literature as reflectance band depths (ΔR), were calculated from recorded reflectance spectra. Feature anomalies were compared with paired water quality parameters (WQPs). Anomalies were calculated by subtracting the observed reflectance magnitude at the center of the feature (R_{center}) from the interpolated reflectance (R_{int}) as estimated by a line connecting points on the spectral continuum to the left (R_{left}, at wavelength λ_{left}) and right (R_{right}, at wavelength λ_{right}) of the feature (Kokaly and Clark, 1999). That is:

$$R_{int} = \frac{R_{left} - R_{right}}{\lambda_{left} - \lambda_{right}} * (\lambda_{center} - \lambda_{left}) + R_{left} \tag{1}$$

$$\Delta R = R_{int} - R_{center} \tag{2}$$

Remote sensing algorithms can then be fitted to this feature, retrieving other statistically correlated parameters that co-vary with the mechanism of light absorption. Following ΔR calculations, regression analysis was performed on experimental data comparing ΔR to measured WQPs to identify correlations and optically active wastewater constituents. Correlations of all paired water quality measurements with spectral feature anomalies are presented both in the Results (Fig. 5) and Supplementary Materials (Tables S3, S4, S5, S6).

Experiment reflectance spectra were convolved to multispectral resolution for ten common satellite sensors (Sentinel-2, Planet SuperDove, Planet Dove, Worldview 2, Worldview 3, Worldview 4, Landsat 8,

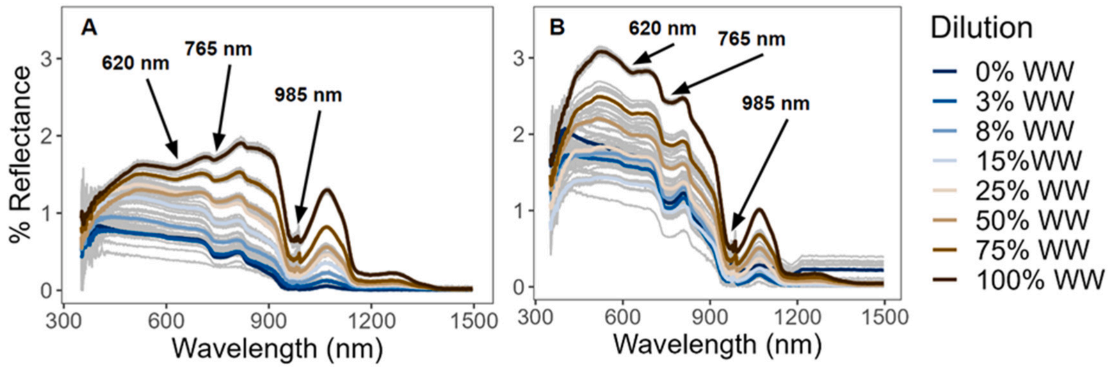

Fig. 3. (A) Reflectance spectra of sample dilutions of wastewater (WW, brown) to seawater (SW, blue) measured on 26 October 2023. (B) Reflectance spectra of sample WW to SW dilutions measured on 14 February 2024. Mean reflectance spectra are plotted in color. Of note, spectra were collected in a shallow matte black container; the container's optical properties contribute to observed reflectances and magnify forward scattering of the medium.

Geoeye, Ikonos, Quickbird) to assess if spectral features were robust to changes in spectral resolution. Δ*R* calculations were then repeated for convolved spectra and compared to WQPs. All correlations for convolved spectra are presented in the Supplementary Materials (Tables S3, S4, S5, S6).

3.3. Field and imagery comparison

To verify if spectral features measured in-lab were also present *in situ*, experimental reflectance spectra were compared to reflectance measurements from a spectroradiometer deployed in the Tijuana Estuary. Starting on 26 May 2022, a GybeSensor™ spectroradiometer was deployed in the Tijuana Estuary (Fig. 1), recording reflectance data at 15-min intervals from 400 to 800 nm. Strict quality assurance flags are provided with the data to screen for cloud cover, unfavorable illumination conditions, and other potential problems. Spectra were retrieved from a period of known wastewater plume conditions from 25 March 2023 to 26 March 2023. *In situ* spectra were then compared to experiment spectra, identifying common features between the two datasets.

Experiment data were further compared with reflectance spectra from both Sentinel-2 multispectral imagery and the Earth Surface Mineral Dust Source Investigation (EMIT) hyperspectral imagery. Operated by the European Space Agency, a constellation of two Sentinel-2 sensors work in tandem; Sentinel-2A was launched 23 June 2015 and Sentinel-2B was launched 7 March 2017. Sentinel-2 sensors measure 13 bands of variable spatial resolutions (10, 20, 60 m). EMIT was launched on 14 July 2022 and has been operating aboard the International Space Station. The sensor collects data from 380 to 2500 nm with 7.4 nm sampling at a spatial resolution of 60 m and a variable temporal revisit and overpass time. Although EMIT's primary goal is to map concentrations of Earth's mineral dust sources, its high spectral resolution and fidelity make it well-suited for water quality applications and science objectives. In this study, we examine Sentinel-2 and EMIT surface reflectance imagery capturing a known wastewater plume near the mouth of the Tijuana River on 24 March 2023 and 25 March 2023. Imagery were acquired through NASA's Earthdata Cloud platform and ESA's Copernicus Browser. Reflectance spectra were compared for pixels within the wastewater plume *versus* several other regions of interest, including within the open ocean.

To visualize the distribution of wastewater in relation to its 620 nm spectral dependency (see Results), the Fluorescence Line Height (FLH) for the 650 nm positive excursion wavelength was calculated using EMIT reflectance data following Xing et al., 2007. Similar to Δ*R*, FLH is computed from the difference between the value at a reflectance peak (*i. e.* 650 nm) and the interpolated reflectance determined from the adjacent reflectance minima. For purposes of mapping wastewater in EMIT imagery, FLH is a more robust metric than Δ*R* to optical complexity at red wavelengths, which can bias Δ*R* values independently of the 620 nm feature (Fig. S4).

$$\mathrm{FLH}\ (650) = R_{650} - \left[R_{670} + \frac{670-650}{670-620} * (R_{620} - R_{670})\right]$$

4. Results

4.1. Wastewater optical properties

For both experiments, a spectral trough feature centered near 620 nm is characteristic of high wastewater concentrations (Fig. 3). In pure and near-pure seawater dilutions, all measured spectra are slightly decreasing from 400 to 700 nm. Once the samples reach approximately 50 % wastewater concentration, a distinct trough feature is observed, centered near 620 nm. For both sampling dates, the depth of this feature increases as the concentration of wastewater increases. Generally, increasing wastewater concentrations also results in a steeper spectral slope at short (300–500 nm) wavelengths. Strong absorption from 300 to 500 nm is characteristic of high CDOM concentrations, though poor signal strength at these high energy wavelengths may decrease the applicability of this feature for model development. Regardless, the depth of this 620 nm feature increases as wastewater concentration increases and may be a reasonable predictor of co-varying water quality parameters.

Additional absorption features centered near 765 and 985 nm are observed at high wastewater concentrations (Fig. 3). 765 nm absorption is present in pure seawater concentrations, the depth of which increases gradually as wastewater concentrations increase. 765 nm absorption and overall high NIR absorption are characteristic of liquid water (Curcio and Petty, 1951). As such, this is likely an inherent property of the distal seawater, not wastewater. This is additionally true for the observed 985 nm absorption feature (Curcio and Petty, 1951). Further, reflectance signals in the NIR region are often screened out during atmospheric correction due to high atmospheric water vapor absorption (Smith and Newnham, 2001). While the 765 and 985 nm features are likely inherent to seawater and not characteristic of Tijuana River wastewater, potential relationships are still explored in analyses along with the 620 nm feature. Of note, the downwelling irradiance of the tungsten halogen lamp peaks in the NIR at approximately 1000–1100 nm (Fig. S1). Multiple scattering within the shallow container likely elevates signal in the red and NIR regions. The reflectance of the vessel itself is spectrally flat from 550 to 2500 nm, with a small reflectance peak centered near 400 nm (Fig. 4).

4.2. Correlation to water quality parameters

Most measured water quality parameters were approximately linearly correlated with the reflectance feature anomaly centered near 620

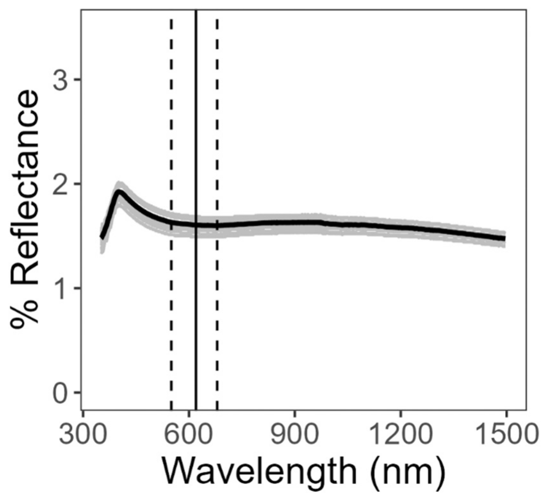

Fig. 4. Reflectance spectra of the matte black container used in spectral data collection. Spectra are approximately flat across most of the VSWIR range, with one peak at 450 nm and a maximum reflectance of approximately 2 %. Reflectance variability in the range of the 620 nm absorption feature is observed to be <0.1 %. The 620 nm feature center (solid) and breadth (dashed) are indicated using vertical lines.

nm (Fig. 5). As reflectance ΔR increases, percent wastewater, CDOM, tryptophan, and *Enterococcus* concentrations all increase approximately linearly. With the exception of tryptophan, parameters also followed similar linear trends between both experiments. Electric conductivity (EC) in mS/cm decreased approximately linearly with feature anomaly and with similar trends between experiments. COD, DOC, and TDN (see Supplementary materials, Tables S3, S4, S5, S6) also all increased approximately linearly with depth. Not all parameters followed strong linear relationships; turbidity was largely uncorrelated with feature depth. Additionally, *E. coli* concentrations and total coliforms (see Supplementary Materials) had weaker correlations overall with 620 nm absorption. All water quality measurements and their correlations with Δ*R* are present in the Supplementary Materials (Tables S1, S2, S3, S4, S5, S6).

4.3. Simulation of multispectral resolution

Experiment reflectance spectra were convolved to the resolution of ten common multispectral satellite sensors. Overall, high correlations between ΔR at 620 nm and WQPs were retained, even as spectral resolution decreased (Fig. 6). Sensors with eight or more bands in the VSWIR region (*i.e.* Sentinel 2, Planet SuperDove (P8), WorldView 2, and WorldView 3) maintained high correlation ($R^2 > 0.90$) between 620 nm anomalies and WQPs for all parameters except bacterial counts (*i.e. Enterococcus*, *E. coli*, total coliforms). In contrast, four band VNIR sensors (*i.e.* Planet 4-band (P4), Quickbird, Ikonos, and Geoeye) had a lower correlation due to a lack of bands centered around 620 nm to capture this feature. This was particularly the case for the February experiment, when reflectance spectra had a narrower wavelength range for the 620 nm feature compared to October spectra. The 620 nm feature was more likely to be captured with four band resolution for October spectra than February, with R^2 values for February spectra ranging from as low as 0.54 to a maximum of 0.75. Multispectral sensors with eight VNIR bands were thus found to effectively capture the 620 nm feature, but multispectral sensors with 4 VNIR bands showed substantially reduced performance.

For 765 and 985 nm absorption, correlations were comparatively weaker and more variable than at 620 nm. Four band sensors are unable to capture the 765 nm feature, as the closest bands which would capture the 765 nm redundantly overlap with those of the 620 nm feature. For VSWIR sensors, the 765 nm feature is observed, though correlations between ΔR and WQPs are lower for each combination of sensor and WQP than at 620 nm. In all cases, sensor resolutions do not record reflectance measurements around the 985 nm absorption feature. This is likely due to high absorption by atmospheric water vapor occurring at

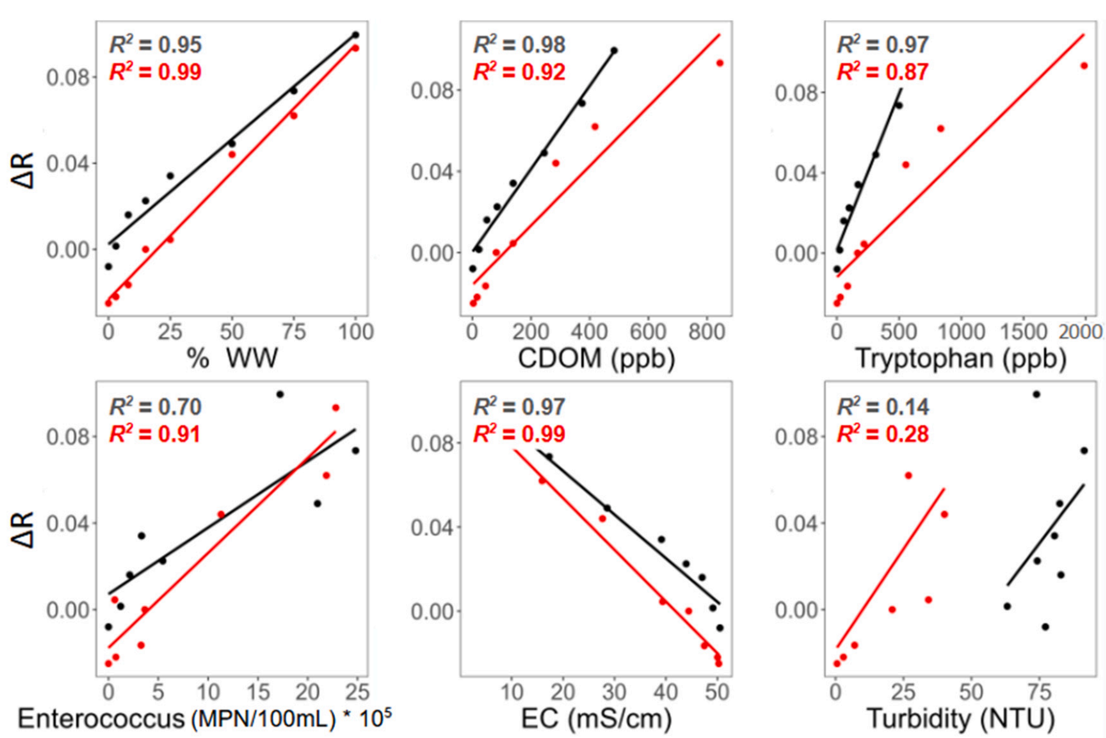

Fig. 5. Relationship between 620 nm reflectance anomalies and percent wastewater, CDOM, tryptophan, *Enterococcus* concentrations, electrical conductivity (EC), and turbidity for the 10/26/2023 (black) and 02/14/2024 (red) experiments. In most cases, water quality parameters are highly correlated with 620 nm absorption, and correlations follow similar linear trends for both experiment replicates.

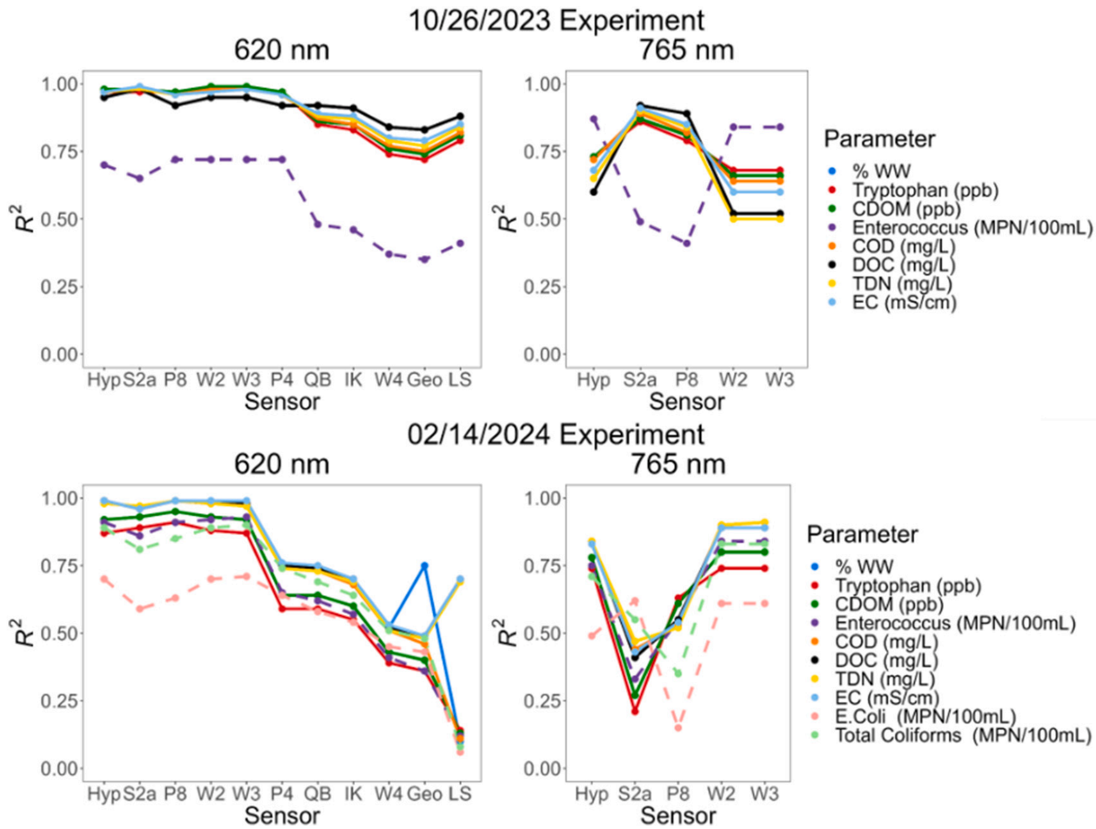

Fig. 6. R2 values for 620 nm and 765 nm band depths as a predictor of various WQPs using convolved experiment spectra. Experiment reflectance spectra were convolved to the spectral response functions of ten common multispectral satellite sensors and used for regression analysis. Sensors with eight or more VNIR bands (i.e. Sentinel 2, Planet SuperDove, WorldView 2, Worldview 3) predominantly retained the 620 nm absorption feature and maintained high correlation, while four band sensors (i.e. Planet 4-band (P4), Quickbird, Ikonos, GeoEye) degraded in performance. Generally, 620 nm band depths were a stronger predictor of WQPs than 765 nm band depths.

these NIR wavelengths, either resulting in a noisy measurement or screening out by an atmospheric correction algorithm.

4.4. In situ and imagery comparisons

The 620 nm feature, which was present in both hyperspectral and simulated multispectral reflectance spectra, is also present *in situ* (Fig. 7B). *In situ* spectra were retrieved during periods of known high and low wastewater discharge (1.68 × 10^6 m^3 from 10:00 25 March 2023 to 15:45 26 March 2023, 0 m^3 from 10:00 to 12:15 02 July 2023). Discharge estimates were obtained from the International Boundary and Water Commission Tijuana River Discharge Flow Gage. Wastewater polluted spectra had three absorption features from 400 to 800 nm, centered at 620, 675, and 765 nm. The 620 and 765 nm features are consistent with the experiment reflectance spectra (Fig. 7A), suggesting these features replicate under high wastewater conditions and may be suitable for algorithm development using *in situ* reflectance data. The additional 675 nm feature is consistent with the well-documented absorption of Chlorophyll-a and likely indicates detectable chlorophyll. Polluted spectra had high spectral shape variability corresponding to rapid changes in sediment suspension, chlorophyll, CDOM, and more; even so, all three absorption features are present in polluted spectra under diverse environmental conditions. Of note, the sampling period of the deployed spectroradiometer is characterized by high near-continuous wastewater discharge, and it may be argued that no "pure, unpolluted" seawater spectrum is present. Nevertheless, there remains a marked difference in 620 nm feature presence under high and low wastewater discharge conditions.

The 620 nm feature is also observed in hyperspectral satellite resolution but not in multispectral (Fig. 7). EMIT imagery shows absorption features at 620, 675, and 765 nm in reflectance spectra that match those observed both *in situ* and in the experiment. These three features are not present in seawater reflectance spectra, which are dominantly spectrally flat from 600 to 800 nm. In image spectra, 765 nm absorption is significantly deeper compared to *in situ* and experiment spectra. Seawater is well documented to have high absorption at red and NIR wavelengths, likely accounting for the 765 nm absorption feature. The positive excursion wavelength of the 620 nm feature shifted to 647 nm compared to experiment reflectance spectra, which had an excursion wavelength of 685 and 710 nm.

Of note, the mediums in which these reflectance data were collected differ among experiment, *in situ*, and image spectra. Experiment spectra were recorded in a shallow matte black container with high internal scattering, *in situ* spectra were recorded above a shallow (<2 m), optically variable water column, and image spectra were recorded over optically deep pixels. The reflectance of the container or benthos likely accounts for much of the variability in spectral shapes and magnitudes, along with differences in sediment loading, tidal variability, and myriad other environmental factors. Regardless of these different mediums and environmental conditions, the 620 nm feature is present in all three sets of spectral data under high wastewater conditions.

4.5. Plume mapping demonstration

Under known wastewater plume conditions, the 620 nm trough feature is observed in EMIT imagery at the mouth of the Tijuana River Estuary, and the feature flattens with distance away from the plume source (Figs. 8A, 9A). EMIT imagery captures a plume of wastewater

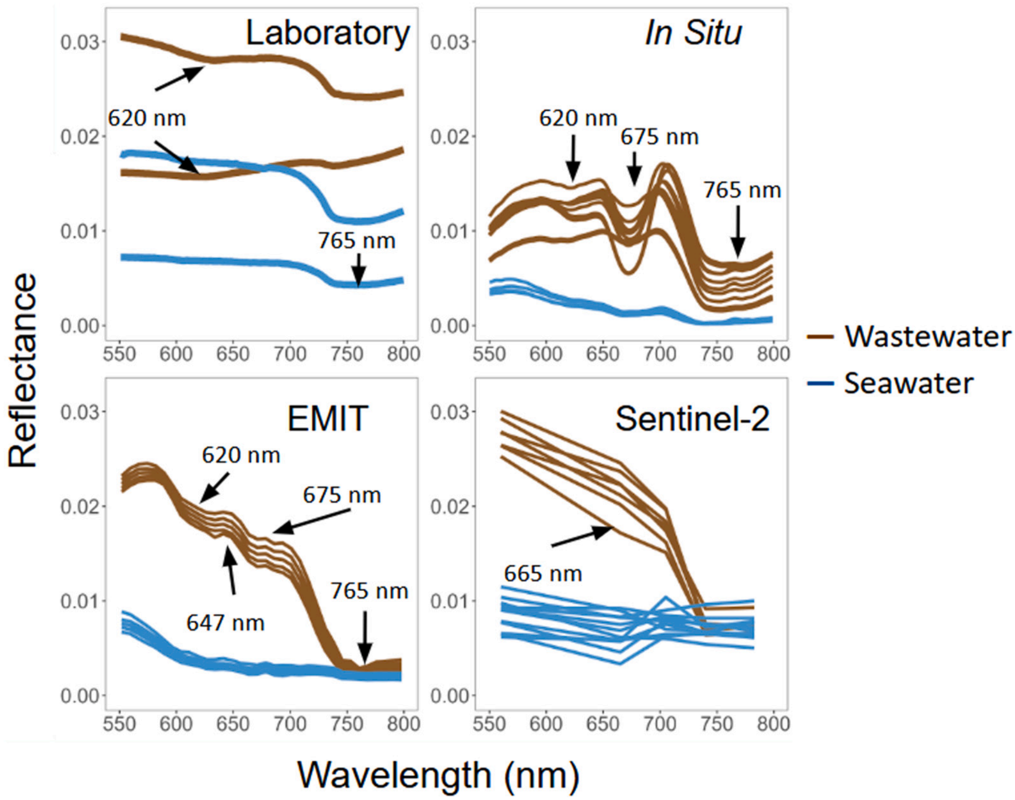

Fig. 7. (A) Laboratory reflectance spectra of seawater and wastewater from 550 to 800 nm collected on 26 October 2023 and 14 February 2024. (B) *In situ* reflectance spectra retrieved from a field deployed spectroradiometer during a period of known high wastewater discharge (1.68×10^6 m^3 from 10:00 25 March 2023 to 15:45 26 March 20233) and low discharge (0 m^3 from 10:00 to 12:15 02 July 2023). (C) EMIT image reflectance spectra of open ocean seawater and of a known wastewater plume in the Tijuana Estuary; imagery acquired on 25 March 2023. (D) Sentinel-2 image reflectance spectra of open ocean seawater and a known wastewater plume; imagery acquired on 24 March 2023. While not present in Sentinel-2 multispectral imagery, 620 nm absorption is present in laboratory, *in situ*, and hyperspectral image spectra and greatest under high wastewater conditions.

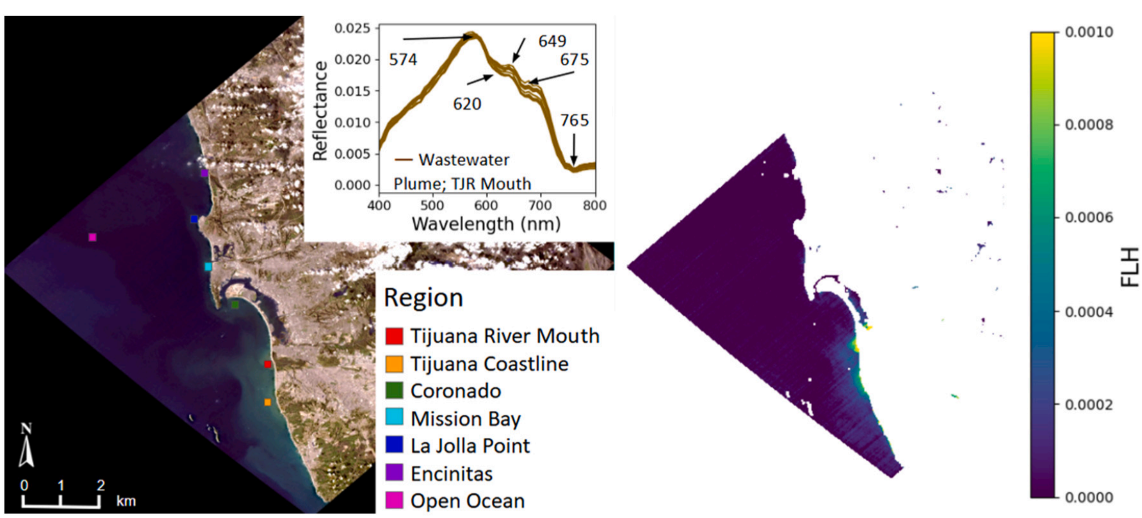

Fig. 8. (A) True color EMIT hyperspectral satellite image covering a known wastewater plume on 25 March 2023. (B) Fluorescence Line Height (FLH) at 650 nm calculated from EMIT reflectance imagery. FLH is greatest at the Tijuana River Estuary and decreases with distance from the estuary mouth.

discharge (on the order of 1.68×10^6 m^3 from 10:00 25 March 2023 to 15:45 26 March 2023) which is expelled from the mouth of the Tijuana River and exported southward (Fig.8A). FLH values of the 650 nm shoulder reflectance peak follow the spatial distribution of this plume (Fig. 8B). FLH values are greatest in magnitude at the river mouth and decrease with distance (Fig. 9B), suggesting a coupled distribution of wastewater and its 620 nm spectral dependency. While further work is necessary to parameterize remote sensing algorithms leveraging this 620–650 nm feature, this demonstration is highly encouraging for remote monitoring of water quality in this region.

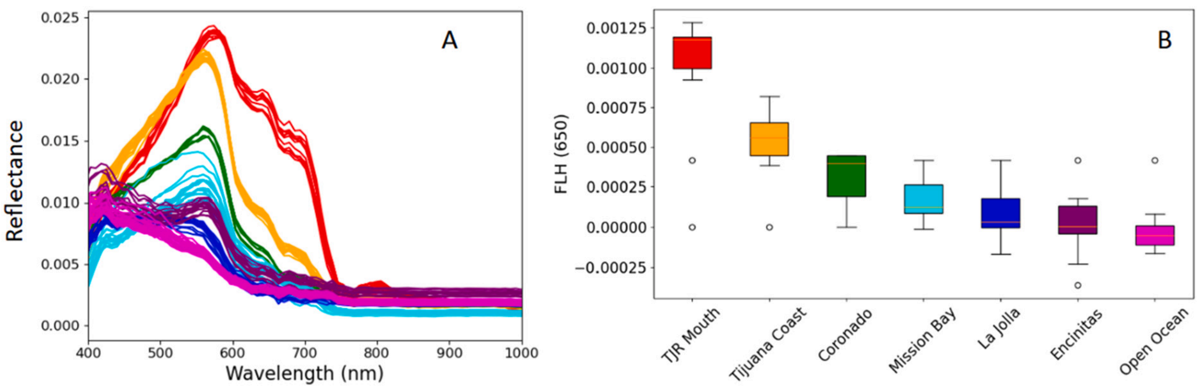

Fig. 9. (A) Reflectance spectra from select regions off the San Diego-Tijuana coastline in EMIT hyperspectral satellite imagery. (B) Fluorescence Line Height (FLH) values for panel A spectra. FLH is greatest at the mouth of the Tijuana River Estuary and decreases with distance from the estuary.

5. Discussion

5.1. 620 nm feature as a water quality indicator

We characterized the spectral properties of untreated wastewater in laboratory experiments, field spectrometers, and hyperspectral satellite imagery. In wastewater addition experiments, we observed a distinct spectral feature centered near 620 nm in high wastewater concentrations. The 620 nm feature correlated strongly with water quality constituents of interest, including bacterial counts. While additional absorption occurs centered at 765 and 985 nm, the 765 nm feature retained weaker correlation and was less robust to loss of spectral resolution than the 620 nm feature (Fig. 6). Furthermore, 765 nm absorption is a well-documented property of pure seawater; thus, it is likely not characteristic of wastewater itself. Strong absorption from atmospheric water vapor hinders satellite observation of reflectance around 985 nm, limiting the applicability of this feature for remote sensing modeling. Our results suggest that 620 nm feature may be both characteristic of high wastewater concentrations and suitable to inform algorithm development for wastewater monitoring in this system.

While the 620 nm feature was retained by experiment reflectance spectra convolved to 8 band-VNIR satellite sensors (Fig. 6), the feature was not observed in actual Sentinel-2 reflectance products. Generally, linear relationships between water quality parameters and the 620 nm absorption feature were strongly retained with 8-band VSWIR sensors, particularly for those with bands fitted within ±20 nm of 620. Four-band VNIR sensors degraded the correlation between ΔR and WQPs, as limited spectral resolution results in a >100 nm window being used for calculation, effectively losing the absorption feature. In the Tijuana River environment, however, an additional reflectance peak centered near 650 nm is observed in *in situ* radiometry and hyperspectral EMIT imagery (Fig. 7). This elevates observed reflectance in the 665 nm band of Sentinel-2 imagery (Fig. 7D). This suggests that enhanced hyperspectral resolution is necessary to reliably characterize wastewater distribution in the Tijuana River Estuary.

Reflectance anomalies at 620 nm had a particularly strong correlation with CDOM and tryptophan concentrations, two critical indicators of water quality. These strong correlations are consistent in both spectroscopic and 8-band VNIR multispectral resolutions (Fig. 6). We recognize that the reflectance over the range of wavelengths measured here (400–1200 nm) are not directly measuring TRP or WQPs (bacteria, conductivity), but rather likely measure other optically active constituents that co-vary with TRP and bacteria. The relationships between optically active compounds and WQPs of interest may vary by location and over time, requiring further experimentation and field data collection. Furthermore, there exist published relationships between tryptophan concentrations and aquatic bacterial parameters (Sorensen et al., 2015; Sorensen et al., 2020; Ward et al., 2021). A tiered remote sensing approach could be applied by first retrieving CDOM and tryptophan concentrations using algorithms tuned to 620 nm absorption, then deriving bacterial parameters from retrieved tryptophan using published relationships.

5.2. Optical sources of 620 nm feature

While many WQPs including CDOM and tryptophan are highly correlated with the 620 nm feature, this does not rule these variables as the specific mechanism of absorption. Rather, we hypothesize the source of this feature to be another pigment or compound that is highly associated with wastewater presence and covaries with the presented WQPs. Our hypotheses for this mechanism are presented below, along with suggestions for future work to identify the source of 620 nm absorption in this wastewater-polluted system.

Phycocyanin, an accessory pigment commonly found in cyanobacteria, exhibits high absorption centered at 620 nm and is a highly plausible mechanism in this system (Simis et al., 2005; Dominguez Gómez et al., 2008; Simis and Kauko, 2012). Under high concentrations of cyanobacteria, a reflectance peak centered near 650 nm can be observed. Kudela et al. (2015) hypothesizes this peak to result from adjacent absorption features of phycocyanin and chlorophyll-a at 620 and 675 nm respectively. This feature is also observed across diverse coastal and inland water bodies under high concentrations of cyanobacteria (Spyrakos et al., 2018; Lehmann et al., 2023). Common phycocyanin-producing genera have been abundantly detected in the Tijuana River Estuary (Tatters et al., 2017). It is also well documented that cyanobacterial blooms form in wastewater treatment facilities due to optimal eutrophic conditions and long residence times (*e.g.* Shanthala et al., 2009; D'Alessandro et al., 2020; Romanis et al., 2021), and in many cases, cyanobacteria are deliberately employed as a form of bioremediation to remove nutrients and secondary organic pollutants (*e.g.* de la Noüe and Bassères, 1989; Laliberté et al., 1997).

We propose that when effluent wastewater is discharged into the Tijuana River system and the wastewater plume mixes and dilutes, so too do coupled cyanobacterial concentrations and their corresponding 620 nm absorption feature. Through this, phycocyanin and its 620 nm absorption covary with wastewater presence and its corresponding water quality parameters, acting as a tracer of plume presence as the wastewater mass travels through the estuary system. Of note, this is an empirical relationship built on covarying wastewater constituents specific to the Tijuana River Estuary system. Future work is necessary to validate if similar relationships exist among other wastewater contaminated coastal systems, and synthesis of these disparate local studies would be necessary to parameterize an eventual global algorithm. Furthermore, while phycocyanin is a strong candidate, further paired spectral, pigment, and absorption analyses are necessary to isolate the physical source of 620 nm absorption, such as through high-performance liquid chromatography (HPLC) or an AC-S spectral absorption and attenuation sensor.

Chlorophyll fluorescence emission is generally acknowledged to occur in the 650 to 800 nm wavelength range (Santabarbara et al., 2020). The shoulder wavelengths of the 620 nm spectral feature were 710 nm in the October experiment and 685 nm in the February experiment (Fig. 3), indeed coinciding with expectations of maximum emission wavelengths of chlorophyll fluorescence are from 685 to 710 nm (Santabarbara et al., 2020, Fig. 10). However, several aspects of the 620 nm spectral feature we observe are inconsistent with the expectations associated with a pure chlorophyll fluorescence signal. First, the chlorophyll *a*bsorption feature at 675 nm was not observed in lab spectra from either experiment — but unlike experiment spectra, the 675 nm chlorophyll *a*bsorption is present in *in situ* reflectance spectra and in hyperspectral satellite imagery (Figs. 7, 8). Further, the wastewater samples used in laboratory experiments were collected in the sunlight-blocked conditions of both the wastewater treatment facility and during transit to the laboratory. It is reasonable to expect that no meaningful selective pressure for photoautotrophy should exist under such conditions. The absence of the 675 nm chlorophyll absorption in the lab spectra, and its presence in the field and satellite spectra, is thus consistent with the onset of eutrophication as the water progresses through the estuary and coastal ocean.

In contrast to these observable and explainable differences between laboratory and field spectra in the 675 nm chlorophyll absorption, the 620 nm spectral feature remains remarkably consistent throughout laboratory, *in situ*, and image spectra. The consistency of the 620 nm feature across observation conditions, combined with both the differences in the 675 nm feature and the sunlight-excluded conditions of the sewage system and lab, limit the plausibility of a simple explanation by a chlorophyll source. There are, however, mixotrophic cyanobacteria which persist in wastewater treatment facilities and can break down organic pollutants (Pittman et al., 2011; Subashchandrabose et al., 2013). More investigation is clearly needed to fully document the spatial and temporal prevalence of this source, and characterize its biochemical origin(s).

One potential, highly undercharacterized mechanism for the 620 nm feature is CDOM fluorescence. Hawes (1992) presents measured fluorescence quantum efficiencies for excitation wavelengths between 310 and 470 nm and emission wavelengths from 320 to 700 nm. Indeed, excitation wavelengths in the UV-A and blue visible ranges may yield fluorescence emission in the 600 nm range, possibly accounting for one of the excursion wavelengths of the 620 nm feature. However, CDOM fluorescence remains heavily under characterized in the aquatic optics literature. While many studies characterize CDOM using fluorescence excitation emission matrices (*e.g.* Li et al., 2022), these matrices present relative differences and are not direct measurements of fluorescence quantum efficiencies. As such, Hawes (1992) presents one of, if not the only measurements of CDOM fluorescent quantum efficiency as of time of writing (Mobley, 1999). Future work is necessary to characterize the spectral dependencies of CDOM fluorescence and validate the findings of Hawes (1992), and wastewater polluted water bodies may prove to be an effective system for this purpose.

Regardless of the biophysical mechanism, spectral dependency at 620 nm is empirically observed in our laboratory experiments to be highly correlated with CDOM, tryptophan, COD, DOC, and more WQPs, both at hyperspectral and multispectral resolution. It is thus plausible that this feature might be leveraged to regionally tune remote sensing algorithms for wastewater management in the Tijuana River system.

While this 620 nm feature is observed under diverse environmental and observational conditions, the development of a regional algorithm from our experimental data is limited by internal scattering of the container and of the wide variability of Tijuana River wastewater. In the wastewater addition experiments, the downwelling irradiance of the tungsten halogen lamp increases exponentially in the red and near infrared, peaking between 1000 and 1100 nm. High scattering within the shallow, matte black container likely amplifies forward scattering and elevates signal in the red and NIR regions. While the observational scheme used in this study was the result of managing hazardous untreated wastewater, parameterization of a regional algorithm will need to account for this error if tuned to the experimental reflectance data collected in this study. Furthermore, the effluent wastewater present in the Tijuana River system contains highly variable chemical and microbial constituents across dynamic hydrologic conditions. Future work is necessary to assess how the 620 nm spectral dependency varies across space and time in this system, and greater synthesis studies would be necessary to assess if this feature may be leveraged in similarly polluted coastal aquatic systems.

5.3. Future applications

Our findings provide the backbone for future projects to develop systematic implementation and production of remote sensing derived wastewater plume maps that also estimate associated water quality parameters such as bacterial concentrations in this system. The ability to do so fills a critical gap in our ability to study how wastewater plumes

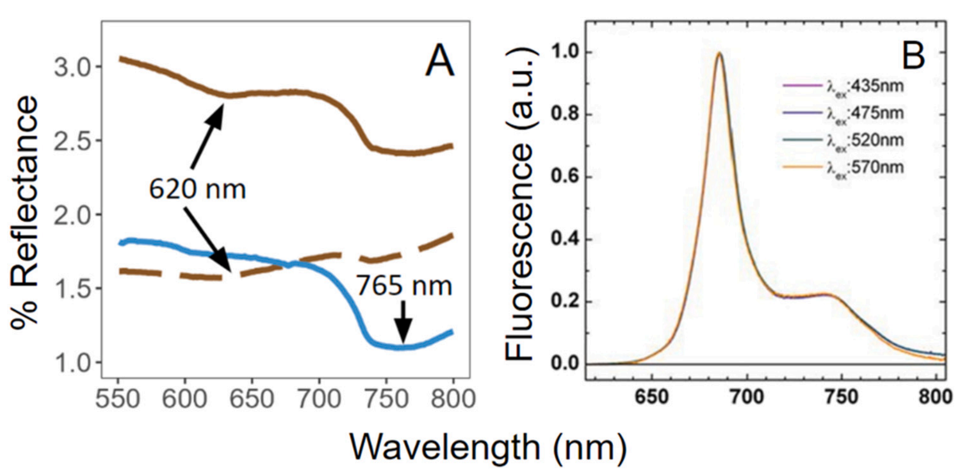

Fig. 10. (A) Laboratory reflectance spectra of pure seawater and wastewater from 550 to 800 nm collected on 10/26/2023 (dashed) and 02/14/2024 (solid). (B) Fluorescence emission spectra for varying excitation wavelengths for chlorophyte *Chlorella sorokinia*. Figure adapted from Santabarbara et al. (2020) and Mobley (1999) under a Creative Commons License. While the positive excursion wavelengths of the 620 nm feature (685 nm in February, 710 nm in October) overlap with the wavelengths of maximum fluorescence emission, experiment spectra lack a characteristic 675 nm chlorophyll-a absorption feature.

impact regional biodiversity, local economies and public health at varying spatial and temporal scales. In this region, modeling approaches and *in situ* sampling are the primary means to estimate plume evolution and spatial extent but cannot resolve nearshore processes and conditions. The scaling of this work to spaceborne assets will allow better understanding of discharge events, extent, and migration, particularly for nearshore conditions (<1 km). Here, we provide a demonstration of wastewater plume mapping by leveraging FLH at 650 nm; future studies may expand upon this and parameterize an algorithm for remote retrievals of regional water quality.

Moreover, the value of this work extends beyond local applications, particularly within the context of UN Sustainable Development Goals. It provides unique value to areas that are impacted by transboundary water pollution issues both in coastal and freshwater aquatic settings and has the potential to support the global agenda for clean water and sanitation (UN SDG Goal 6), especially in areas where on the ground sampling, data and resource sharing, are limited. It should also be noted that because of limited ground sampling and that regional tuning is needed, that initial applications of spectrally based mapping of wastewater plumes should be limited to screening and assessment, rather than direct characterization of health/epidemiological risks and may enhance monitoring in regions that are experiencing chronic wastewater spills into coastal regions. By providing a consistent and reliable data record through repeat measurements, remote sensing technologies can significantly contribute to achieving these goals. Thereby addressing one of the most pressing environmental challenges of our time.

6. Conclusions

This study investigated the potential to map and monitor water quality in the Tijuana River Estuary through field and satellite imaging spectroscopy. To meet this aim, reflectance spectra of wastewater-seawater dilutions were recorded and analyzed. Our key findings are as follows:

1) Under high wastewater conditions, a 620 nm spectral dependency is observed.
2) 620 nm absorption depth was highly correlated with paired measurements of water quality parameters (WQPs).
3) When convolved to 8-band VNIR resolution, 620 nm absorption and its correlation to WQPs were retained, but they were not observed in Sentinel-2 satellite imagery.
4) 620 nm absorption is present both *in situ*, with a field-deployed spectroradiometer, and in hyperspectral satellite imagery under known wastewater plume conditions.
5) We hypothesize phycocyanin, a common accessory pigment, to be the physical source of 620 nm absorption.
6) Additional features centered at 765 and 985 nm were also observed. 765 nm absorption likely results from well-documented seawater absorption, while 985 nm is not commonly detectable in satellite sensors due to atmospheric noise.
7) Future remote sensing algorithms may be tuned to 620 nm absorption for routine water quality monitoring in the Tijuana River Estuary.
8) A demonstration of wastewater plume mapping with EMIT imagery is presented, highlighting potential applications of this sensor for water quality applications.

CRediT authorship contribution statement

Eva Scrivner: Writing – review & editing, Writing – original draft, Visualization, Validation, Software, Methodology, Investigation, Formal analysis, Data curation, Conceptualization. **Natalie Mladenov:** Writing – review & editing, Supervision, Resources, Methodology, Investigation, Data curation, Conceptualization. **Trent Biggs:** Writing – review & editing, Methodology, Investigation, Data curation, Conceptualization. **Alexandra Grant:** Writing – review & editing, Methodology, Formal analysis, Data curation. **Elise Piazza:** Formal analysis, Data curation. **Stephany Garcia:** Methodology, Investigation, Data curation. **Christine M. Lee:** Writing – review & editing, Supervision, Methodology, Investigation, Funding acquisition, Conceptualization. **Christiana Ade:** Writing – review & editing, Methodology, Investigation, Formal analysis. **Nick Tufillaro:** Writing – review & editing, Methodology, Investigation. **Philipp Grötsch:** Writing – review & editing, Software, Methodology, Investigation, Formal analysis. **Omar Zurita:** Methodology, Data curation. **Benjamin Holt:** Writing – review & editing, Supervision, Funding acquisition, Conceptualization. **Daniel Sousa:** Writing – review & editing, Writing – original draft, Supervision, Methodology, Investigation, Funding acquisition, Formal analysis, Data curation, Conceptualization.

Declaration of competing interest

The authors declare the following financial interests/personal relationships which may be considered as potential competing interests: Nick Tufillaro reports a relationship with Gybe that includes: employment. Philipp Grotsch reports a relationship with Gybe that includes: employment. Omar Zurita reports a relationship with Gybe that includes: employment. If there are other authors, they declare that they have no known competing financial interests or personal relationships that could have appeared to influence the work reported in this paper.

Acknowledgments

We gratefully acknowledge funding from the NASA Remote Sensing of Water Quality Program (Grant #80NSSC22K0907) and the NASA Applications-Oriented Augmentations for Research and Analysis Program (Grant #80NSSC23K1460). DS also acknowledges funding from the USDA NIFA Sustainable Agroecosystems Program (Grant #2022-67019-36397), the USDA AFRI Rapid Response to Extreme Weather Events Across Food and Agricultural Systems Program (Grant #2023-68016-40683), the NASA Land-Cover/Land Use Change Program (Grant #NNH21ZDA001N-LCLUC), the NASA EMIT Science and Applications Team (Grant #80NSSC24K0861), the NASA Commercial Smallsat Data Analysis Program (Grant #80NSSC24K0052), the NASA FireSense Airborne Science Program (Grant #80NSSC24K0145), the California Climate Action Seed Award Program, and the NSF Signals in the Soil Program (Award #2226649). We acknowledge funding from the U.S. Environmental Protection Agency (PR-ORD-21-01804) and the J.W. Sefton Foundation. Stephany Garcia was supported in part by the National Oceanic and Atmospheric Administration (NOAA) Educational Partnership Program/Minority-Serving Institutions (EPP/MSI) award NA22SEC4810016 to the Center for Earth System Sciences and Remote Sensing Technologies II (CESSRST II). This research was carried out in part at the Jet Propulsion Laboratory, California Institute of Technology, under contract with the National Aeronautics and Space Administration. We also gratefully acknowledge the European Space Agency Copernicus and NASA Earthdata browsers for enabling open data access that made this work possible.

Appendix A. Supplementary data

Supplementary data to this article can be found online at https://doi.org/10.1016/j.scitotenv.2025.179598.

Data availability

Data will be made available on request.

References

Arana, I., Seco, C., Epelde, K., Muela, A., Fernández-Astorga, A., Barcina, I., 2004. Relationships between *Escherichia coli* cells and the surrounding medium during survival processes. Antonie Van Leeuwenhoek 86, 189–199. https://doi.org/10.1023/B:ANTO.0000036146.28808.93.

Aurin, D., Mannino, A., Lary, D.J., 2018. Remote sensing of CDOM, CDOM spectral slope, and dissolved organic carbon in the global ocean. Appl. Sci. (Basel) 8, 2687. https://doi.org/10.3390/app8122687.

Ayad, M., Li, J., Holt, B., Lee, C., 2020. Analysis and classification of stormwater and wastewater runoff from the Tijuana River using remote sensing imagery. Front. Environ. Sci. 8.

Bay, S., Jones, B.H., Schiff, K., Washburn, L., 2003. Water quality impacts of stormwater discharges to Santa Monica Bay. Mar. Environ. Res. 56, 205–223. https://doi.org/10.1016/S0141-1136(02)00331-8.

Bidigare, R., Ondrusek, M., Morrow, J., Kiefer, D., 1990. In-vivo absorption properties of algal pigments. Proc. SPIE 1302. https://doi.org/10.1117/12.21451.

Brando, V.E., Dekker, A.G., 2003. Satellite hyperspectral remote sensing for estimating estuarine and coastal water quality. IEEE Trans. Geosci. Remote Sens. 41, 1378–1387. https://doi.org/10.1109/TGRS.2003.812907.

Bricaud, A., Babin, M., Morel, A., Claustre, H., 1995. Variability in the chlorophyll-specific absorption coefficients of natural phytoplankton: analysis and parameterization. J. Geophys. Res. 100, 13321–13332. https://doi.org/10.1029/95JC00463.

Brivio, P.A., Giardino, C., Zilioli, E., 2001. Validation of satellite data for quality assurance in lake monitoring applications. Sci. Total Environ. 268, 3–18. https://doi.org/10.1016/S0048-9697(00)00693-8.

Calderón-Villarreal, A., Terry, B., Friedman, J., González-Olachea, S.A., Chavez, A., Díaz López, M., Pacheco Bufanda, L., Martinez, C., Medina Ponce, S.E., Cázares-Adame, R., Rochin Bochm, P.F., Kayser, G., Strathdee, S.A., Muñoz Meléndez, G., Holmes, S.M., Bojorquez, I., Los Huertos, M., Bourgois, P., 2022. Deported, homeless, and into the canal: environmental structural violence in the binational Tijuana River. Soc. Sci. Med. 305, 115044. https://doi.org/10.1016/j.socscimed.2022.115044.

California-Mexico Border Relations Council, 2017. 2017 Annual Report of the California-Mexico Border Relations Council.

Cheng, K.H., Jiao, J.J., Luo, X., Yu, S., 2022. Effective coastal *Escherichia coli* monitoring by unmanned aerial vehicles (UAV) thermal infrared images. Water Res. 222, 118900. https://doi.org/10.1016/j.watres.2022.118900.

Ciotti, Á.M., Lewis, M.R., Cullen, J.J., 2002. Assessment of the relationships between dominant cell size in natural phytoplankton communities and the spectral shape of the absorption coefficient. Limnol. Oceanogr. 47, 404–417. https://doi.org/10.4319/lo.2002.47.2.0404.

Coble, P.G., 1996. Characterization of marine and terrestrial DOM in seawater using excitation-emission matrix spectroscopy. Mar. Chem. 51, 325–346. https://doi.org/10.1016/0304-4203(95)00062-3.

Curcio, J.A., Petty, C.C., 1951. The near infrared absorption spectrum of liquid water. J. Opt. Soc. Am. 41, 302–304. https://doi.org/10.1364/JOSA.41.000302.

D'Alessandro, E.B., Nogueira, I.S., Hoffmann, N.K.S.A., 2020. Variability in phytoplankton community structure and influence on stabilization pond functioning. Rev. Ambient. Água 15, e2507. https://doi.org/10.4136/ambi-agua.2507.

Dapkus, R.T., Fryar, A.E., Tobin, B.W., Byrne, D.M., Sarker, S.K., Bettel, L., Fox, J.F., 2023. Utilization of tryptophan-like fluorescence as a proxy for *E. coli* contamination in a mixed-land-use karst basin. Hydrology 10, 74. https://doi.org/10.3390/hydrology10040074.

Dekker, A.G., 1993. Detection of Optical Water Quality Parameters for Entrophic Waters by High Resolution Remote Sensing. Free University, Amsterdam.

DiGiacomo, P.M., Washburn, L., Holt, B., Jones, B.H., 2004. Coastal pollution hazards in southern California observed by SAR imagery: stormwater plumes, wastewater plumes, and natural hydrocarbon seeps. Mar. Pollut. Bull. 49, 1013–1024. https://doi.org/10.1016/j.marpolbul.2004.07.016.

Dominguez Gómez, J., Alonso-Alonso, C., Alonso, A., 2008. Remote sensing as a basic toolbox for monitoring water quality parameters and as a system of surveillance of cyanobacterial harmful algae blooms (SCyanoHABs). In: Presented at the International Geoscience and Remote Sensing Symposium (IGARSS), pp. IV–886. https://doi.org/10.1109/IGARSS.2008.4779865.

Feddersen, F., Boehm, A.B., Giddings, S.N., Wu, X., Liden, D., 2021. Modeling untreated wastewater evolution and swimmer illness for four wastewater infrastructure scenarios in the San Diego-Tijuana (US/MX) border region. GeoHealth 5. https://doi.org/10.1029/2021GH000490 e2021GH000490.

Freitas, F., Dierssen, H.M., 2019. Evaluating the seasonal and decadal performance of red band difference algorithms for chlorophyll in an optically complex estuary with winter and summer blooms. Remote Sens. Environ. 231, 111228. https://doi.org/10.1016/j.rse.2019.111228.

Gemperli, C., 2004. Determination of Water Quality Parameters in Indian Ponds Using Remote Sensing Methods.

George, D.G., 1997. The airborne remote sensing of phytoplankton chlorophyll in the lakes and tarns of the English Lake District. Int. J. Remote Sens. 18, 1961–1975. https://doi.org/10.1080/014311697217972.

Gholizadeh, M.H., Melesse, A.M., Reddi, L., 2016. A comprehensive review on water quality parameters estimation using remote sensing techniques. Sensors 16, 1298. https://doi.org/10.3390/s16081298.

Giardino, C., Brando, V.E., Dekker, A.G., Strömbeck, N., Candiani, G., 2007. Assessment of water quality in Lake Garda (Italy) using Hyperion. Remote Sens. Environ. 109, 183–195. https://doi.org/10.1016/j.rse.2006.12.017.

Gierach, M.M., Holt, B., Trinh, R., Jack Pan, B., Rains, C., 2017. Satellite detection of wastewater diversion plumes in Southern California. Estuar. Coast. Shelf Sci. 186, 171–182. https://doi.org/10.1016/j.ecss.2016.10.012.

Gitelson, A.A., Dall'Olmo, G., Moses, W., Rundquist, D.C., Barrow, T., Fisher, T.R., Gurlin, D., Holz, J., 2008. A simple semi-analytical model for remote estimation of chlorophyll-*a* in turbid waters: validation. Remote Sens. Environ. 112, 3582–3593. https://doi.org/10.1016/j.rse.2008.04.015.

Gitelson, A.A., Gurlin, D., Moses, W.J., Barrow, T., 2009. A bio-optical algorithm for the remote estimation of the chlorophyll-a concentration in case 2 waters. Environ. Res. Lett. 4, 045003. https://doi.org/10.1088/1748-9326/4/4/045003.

Goldman, J.H., Rounds, S.A., Needoba, J.A., 2012. Applications of fluorescence spectroscopy for predicting percent wastewater in an urban stream. Environ. Sci. Technol. 46, 4374–4381. https://doi.org/10.1021/es2041114.

Gordon, H.R., Morel, A.Y., 1983. Remote Assessment of Ocean Color for Interpretation of Satellite Visible Imagery: A Review. Springer Science & Business Media.

Grimes, D., Ford, T., Colwell, R., Baker-Austin, C., Martinez-Urtaza, J., Subramaniam, A., Capone, D., 2014. Viewing marine bacteria, their activity and response to environmental drivers from orbit: satellite remote sensing of bacteria. Microb. Ecol. 67. https://doi.org/10.1007/s00248-013-0363-4.

Grunert, B.K., Mouw, C.B., Ciochetto, A.B., 2018. Characterizing CDOM spectral variability across diverse regions and spectral ranges. Glob. Biogeochem. Cycles 32, 57–77. https://doi.org/10.1002/2017GB005756.

Hawes, S.K., Carder, K.L., Harvey, G.R., 1992. In: Optics XI. SPIE, pp. 212–223. https://doi.org/10.1117/12.140652.

He, B., Oki, K., Wang, Y., Oki, T., 2009. Using remotely sensed imagery to estimate potential annual pollutant loads in river basins. Water Sci. Technol. 60, 2009–2015. https://doi.org/10.2166/wst.2009.596.

Holt, B., Trinh, R., Gierach, M.M., 2017. Stormwater runoff plumes in the Southern California Bight: a comparison study with SAR and MODIS imagery. Mar. Pollut. Bull. 118, 141–154. https://doi.org/10.1016/j.marpolbul.2017.02.040.

Hudson, N., Baker, A., Ward, D., Reynolds, D.M., Brunsdon, C., Carliell-Marquet, C., Browning, S., 2008. Can fluorescence spectrometry be used as a surrogate for the Biochemical Oxygen Demand (BOD) test in water quality assessment? An example from South West England. Sci. Total Environ. 391, 149–158. https://doi.org/10.1016/j.scitotenv.2007.10.054.

International Boundary and Water Commision, 2020. Binational Water Quality Study of the Tijuana River and Adjacent Canyons and Drains.

International Boundary and Water Commision, 2022. Minute No. 328: Sanitation Infrastructure Projects in San Diego.

Jerlov, N.G., 1968. Optical Oceanography. Elsevier Pub. Co., Amsterdam, New York.

Kallio, K., Kutser, T., Hannonen, T., Koponen, S., Pulliainen, J., Vepsäläinen, J., Pyhälahti, T., 2001. Retrieval of water quality from airborne imaging spectrometry of various lake types in different seasons. Sci. Total Environ. 268, 59–77. https://doi.org/10.1016/S0048-9697(00)00685-9.

Kirk, J.T.O., 1976. Yellow substance (gelbstoff) and its contribution to the attenuation of photosynthetically active radiation in some inland and coastal south-eastern Australian waters. Mar. Freshw. Res. 27, 61–71. https://doi.org/10.1071/mf9760061.

Kokaly, R.F., Clark, R.N., 1999. Spectroscopic determination of leaf biochemistry using band-depth analysis of absorption features and stepwise multiple linear regression. Remote Sens. Environ. 67, 267–287. https://doi.org/10.1016/S0034-4257(98)00084-4.

Kudela, R.M., Palacios, S.L., Austerberry, D.C., Accorsi, E.K., Guild, L.S., Torres-Perez, J., 2015. Application of hyperspectral remote sensing to cyanobacterial blooms in inland waters. Remote Sens. Environ. 167, 196–205. https://doi.org/10.1016/j.rse.2015.01.025. Special Issue on the Hyperspectral Infrared Imager (HyspIRI).

Laliberté, G., Lessard, P., de la Noüe, J., Sylvestre, S., 1997. Effect of phosphorus addition on nutrient removal from wastewater with the cyanobacterium *Phormidium bohneri*. Bioresour. Technol. 59, 227–233. https://doi.org/10.1016/S0960-8524(96)00144-7.

Lee, Z., Carder, K.L., Arnone, R.A., 2002. Deriving inherent optical properties from water color: a multiband quasi-analytical algorithm for optically deep waters. Appl. Opt. 41, 5755–5772. https://doi.org/10.1364/AO.41.005755.

Lehmann, M.K., Gurlin, D., Pahlevan, N., Alikas, K., Conroy, T., Anstee, J., Balasubramanian, S.V., Barbosa, C.C.F., Binding, C., Bracher, A., Bresciani, M., Burtner, A., Cao, Z., Dekker, A.G., Di Vittorio, C., Drayson, N., Errera, R.M., Fernandez, V., Ficek, D., Fichot, C.G., Gege, P., Giardino, C., Gitelson, A.A., Greb, S.R., Henderson, H., Higa, H., Rahaghi, A.I., Jamet, C., Jiang, D., Jordan, T., Kangro, K., Kravitz, J.A., Kristoffersen, A.S., Kudela, R., Li, L., Ligi, M., Loisel, H., Lohrenz, S., Ma, R., Maciel, D.A., Malthus, T.J., Matsushita, B., Matthews, M., Minaudo, C., Mishra, D.R., Mishra, S., Moore, T., Moses, W.J., Nguyễn, H., Novo, E.M.L.M., Novoa, S., Odermatt, D., O'Donnell, D.M., Olmanson, L.G., Ondrusek, M., Oppelt, N., Ouillon, S., Pereira Filho, W., Plattner, S., Verdú, A.R., Salem, S.I., Schalles, J.F., Simis, S.G.H., Siswanto, E., Smith, B., Somlai-Schweiger, I., Soppa, M.A., Spyrakos, E., Tessin, E., van der Woerd, H.J., Vander Woude, A., Vandermeulen, R.A., Vantrepotte, V., Wernand, M.R., Werther, M., Young, K., Yue, L., 2023. GLORIA — a globally representative hyperspectral in situ dataset for optical sensing of water quality. Sci. Data 10, 100. https://doi.org/10.1038/s41597-023-01973-y.

Li, Y., Zhang, Y., Li, Z., Wan, J., Dang, C., Fu, J., 2022. Characterization of colored dissolved organic matter in the northeastern South China Sea using EEMs-PARAFAC and absorption spectroscopy. J. Sea Res. 180, 102159. https://doi.org/10.1016/j.seares.2021.102159.

Mannino, A., Russ, M.E., Hooker, S.B., 2008. Algorithm development and validation for satellite-derived distributions of DOC and CDOM in the U.S. Middle Atlantic Bight. J. Geophys. Res. Oceans 113. https://doi.org/10.1029/2007JC004493.

McLamb, F., Feng, Z., Shea, D., Bozinovic, K., Vasquez, M.F., Stransky, C., Gersberg, R. M., Wang, W., Kong, X., Xia, X.-R., Bozinovic, G., 2024. Evidence of transboundary movement of chemicals from Mexico to the U.S. in Tijuana River Estuary sediments. Chemosphere 348, 140749. https://doi.org/10.1016/j.chemosphere.2023.140749.

Mendoza, L.M., Mladenov, N., Kinoshita, A.M., Pinongcos, F., Verbyla, M.E., Gersberg, R., 2020. Fluorescence-based monitoring of anthropogenic pollutant inputs to an urban stream in Southern California, USA. Sci. Total Environ. 718, 137206. https://doi.org/10.1016/j.scitotenv.2020.137206.

Miao-fen, H., Xu-feng, X., Xiao-ping, Q., Wu-yi, Y., Yi-min, Z., 2007. Identification mode of chemical oxygen demand in water based on remotely sensing technique and its application. In: 2007 IEEE International Geoscience and Remote Sensing Symposium. Presented at the 2007 IEEE International Geoscience and Remote Sensing Symposium, pp. 1738–1741. https://doi.org/10.1109/IGARSS.2007.4423154.

Miller, R.L., DelCastillo, C.E., Powell, R.T., DSa, E., Spiering, B., 2002. Mapping CDOM Concentration in Waters Influenced by the Mississippi River Plume.

Mobley, C.D., 1999. Estimation of the remote-sensing reflectance from above-surface measurements. Appl. Opt. 38, 7442–7455. https://doi.org/10.1364/AO.38.007442.

Morgan, B.J., Stocker, M.D., Pachepsky, Y.A., Kim, M.S., 2021. Accuracy and reliability of predictions of *E. coli* concentrations in water of irrigation ponds from drone-based imagery as affected by parameters of the random forest algorithm. In: Sensing for Agriculture and Food Quality and Safety XIII. Presented at the Sensing for Agriculture and Food Quality and Safety XIII, SPIE, pp. 44–54. https://doi.org/10.1117/12.2586220.

Moses, W.J., Gitelson, A.A., Berdnikov, S., Povazhnyy, V., 2009. Estimation of chlorophyll-a concentration in case II waters using MODIS and MERIS data—successes and challenges. Environ. Res. Lett. 4, 045005. https://doi.org/10.1088/1748-9326/4/4/045005.

Myint, S.W., Walker, N.D., 2002. Quantification of surface suspended sediments along a river dominated coast with NOAA AVHRR and SeaWiFS measurements: Louisiana, USA. Int. J. Remote Sens. 23, 3229–3249. https://doi.org/10.1080/01431160110104700.

Nechad, B., Ruddick, K.G., Park, Y., 2010. Calibration and validation of a generic multisensor algorithm for mapping of total suspended matter in turbid waters. Remote Sens. Environ. 114, 854–866. https://doi.org/10.1016/j.rse.2009.11.022.

de la Noüe, J., Bassères, A., 1989. Biotreatment of anaerobically digested swine manure with microalgae. Biol. Wastes 29, 17–31. https://doi.org/10.1016/0269-7483(89)90100-6.

Nowicki, S., deLaurent, Z.R., de Villiers, E.P., Githinji, G., Charles, K.J., 2021. The utility of *Escherichia coli* as a contamination indicator for rural drinking water: evidence from whole genome sequencing. PLoS One 16, e0245910. https://doi.org/10.1371/journal.pone.0245910.

Pittman, J.K., Dean, A.P., Osundeko, O., 2011. The potential of sustainable algal biofuel production using wastewater resources. Bioresource Technol. 102, 17–25. https://doi.org/10.1016/j.biortech.2010.06.035. Special Issue: Biofuels - II: Algal Biofuels and Microbial Fuel Cells.

Randolph, K., Wilson, J., Tedesco, L., Li, L., Pascual, D.L., Soyeux, E., 2008. Hyperspectral remote sensing of cyanobacteria in turbid productive water using optically active pigments, chlorophyll *a* and phycocyanin. Remote Sens. Environ. 112, 4009–4019. https://doi.org/10.1016/j.rse.2008.06.002.

Ritchie, J.C., Cooper, C.M., Schiebe, F.R., 1990. The relationship of MSS and TM digital data with suspended sediments, chlorophyll, and temperature in Moon Lake, Mississippi. Remote Sens. Environ. 33, 137–148. https://doi.org/10.1016/0034-4257(90)90039-O.

Romanis, C.S., Pearson, L.A., Neilan, B.A., 2021. Cyanobacterial blooms in wastewater treatment facilities: significance and emerging monitoring strategies. J. Microbiol. Methods 180, 106123. https://doi.org/10.1016/j.mimet.2020.106123.

Santabarbara, S., Remelli, W., Petrova, A.A., Casazza, A.P., Santabarbara, S., Remelli, W., Petrova, A.A., Casazza, A.P., 2020. Influence of the wavelength of excitation and fluorescence emission detection on the estimation of fluorescence-based physiological parameters in different classes of photosynthetic organisms. In: Fluorescence Methods for Investigation of Living Cells and Microorganisms. IntechOpen. https://doi.org/10.5772/intechopen.93230.

Seyhan, E., Dekker, A., 1986. Application of remote sensing techniques for water quality monitoring. Hydrobiol. Bull. 20, 41–50. https://doi.org/10.1007/BF02291149.

Shanthala, M., Hosmani, S.P., Hosetti, B.B., 2009. Diversity of phytoplanktons in a waste stabilization pond at Shimoga Town, Karnataka State, India. Environ. Monit. Assess. 151, 437–443. https://doi.org/10.1007/s10661-008-0287-5.

Simis, S., Peters, S., Gons, H., 2005. Remote sensing of the cyanobacterial pigment phycocyanin in turbid inland water. Limnol. Oceanogr. 50, 237–245.

Simis, S., Ruiz-Verdu, A., Gómez, J., Peña-Martinez, R., Peters, S., Gons, H., 2006. Influence of phytoplankton pigment composition on remote sensing of cyanobacterial biomass. Remote Sens. Environ. 106, 414–427. https://doi.org/10.1016/j.rse.2006.09.008.

Simis, S.G.H., Kauko, H.M., 2012. In vivo mass-specific absorption spectra of phycobilipigments through selective bleaching. Limnol. Oceanogr. Methods 10, 214–226. https://doi.org/10.4319/lom.2012.10.214.

Smith, K.M., Newnham, D.A., 2001. High-resolution atmospheric absorption by water vapor in the 830–985 nm region: evaluation of spectroscopic databases. Geophys. Res. Lett. 28, 3115–3118. https://doi.org/10.1029/2001GL013155.

Sorensen, J.P.R., Lapworth, D.J., Marchant, B.P., Nkhuwa, D.C.W., Pedley, S., Stuart, M. E., Bell, R.A., Chirwa, M., Kabika, J., Liemisa, M., Chibesa, M., 2015. In-situ tryptophan-like fluorescence: a real-time indicator of faecal contamination in drinking water supplies. Water Res. 81, 38–46. https://doi.org/10.1016/j.watres.2015.05.035.

Sorensen, J.P.R., Carr, A.F., Nayebare, J., Diongue, D.M.L., Pouye, A., Roffo, R., Gwengweya, G., Ward, J.S.T., Kanoti, J., Okotto-Okotto, J., van der Marel, L., Ciric, L., Faye, S.C., Gaye, C.B., Goodall, T., Kulabako, R., Lapworth, D.J., MacDonald, A.M., Monjerezi, M., Olago, D., Owor, M., Read, D.S., Taylor, R.G., 2020. Tryptophan-like and humic-like fluorophores are extracellular in groundwater: implications as real-time faecal indicators. Sci. Rep. 10, 15379. https://doi.org/10.1038/s41598-020-72258-2.

Spyrakos, E., O'Donnell, R., Hunter, P.D., Miller, C., Scott, M., Simis, S.G.H., Neil, C., Barbosa, C.C.F., Binding, C.E., Bradt, S., Bresciani, M., Dall'Olmo, G., Giardino, C., Gitelson, A.A., Kutser, T., Li, L., Matsushita, B., Martinez-Vicente, V., Matthews, M. W., Ogashawara, I., Ruiz-Verdú, A., Schalles, J.F., Tebbs, E., Zhang, Y., Tyler, A.N., 2018. Optical types of inland and coastal waters. Limnol. Oceanogr. 63, 846–870. https://doi.org/10.1002/lno.10674.

Subashchandrabose, S.R., Ramakrishnan, B., Megharaj, M., Venkateswarlu, K., Naidu, R., 2013. Mixotrophic cyanobacteria and microalgae as distinctive biological agents for organic pollutant degradation. Environ. Int. 51, 59–72. https://doi.org/10.1016/j.envint.2012.10.007.

SVC, 2012. HR-1024i/SVC HR 768i User Manual Revision 1.5. Poughkeepsie, New York.

Tatters, A.O., Howard, M.D.A., Nagoda, C., Busse, L., Gellene, A.G., Caron, D.A., 2017. Multiple stressors at the land-sea interface: cyanotoxins at the land-sea interface in the Southern California Bight. Toxins (Basel) 9, 95. https://doi.org/10.3390/toxins9030095.

Tehrani, N.C., D'Sa, E.J., Osburn, C.L., Bianchi, T.S., Schaeffer, B.A., 2013. Chromophoric dissolved organic matter and dissolved organic carbon from Sea-Viewing Wide Field-of-View Sensor (SeaWiFS), Moderate Resolution Imaging Spectroradiometer (MODIS) and MERIS sensors: case study for the northern Gulf of Mexico. Remote Sens. 5, 1439–1464. https://doi.org/10.3390/rs5031439.

Tijuana River National Estuarine Research Reserve, 2020. Goat Canyon Sediment Basins: An Effective Model for Marine Debris Capture in the Tijuana River Watershed.

Visser, S.A., 1984. Seasonal changes in the concentration and colour of humic substances in some aquatic environments. Freshw. Biol. 14, 79–87. https://doi.org/10.1111/j.1365-2427.1984.tb00023.x.

Ward, J.S.T., Lapworth, D.J., Read, D.S., Pedley, S., Banda, S.T., Monjerezi, M., Gwengweya, G., MacDonald, A.M., 2021. Tryptophan-like fluorescence as a high-level screening tool for detecting microbial contamination in drinking water. Sci. Total Environ. 750, 141284. https://doi.org/10.1016/j.scitotenv.2020.141284.

Xing, X.-G., Zhao, D.-Z., Liu, Y.-G., Yang, J.-H., Xiu, P., Wang, L., 2007. An overview of remote sensing of chlorophyll fluorescence. Ocean Sci. J. 42, 49–59. https://doi.org/10.1007/BF03020910.

Zhang, Z., Deng, Z.-Q., Rusch, K.A., Wing, M.G., Chenier, K., 2010. Remote sensing algorithms for estimating *Enterococcus* concentration in coastal Louisiana beaches. In: Presented at the 5th International Conference on Environmental Science and Technology, Houston, TX.